Anal. Chem. **2009,** *81,* 2737–2744

Surface Reaction Limited Model for the Evaluation of Immobilized Enzyme on Planar Surfaces

Cheng-Che Lee,[†] Han-Ping Chiang,[†] Kun-Lin Li,[‡] Fu-Hsiang Ko,[‡] Chien-Ying Su,[§] and Yuh-Shyong Yang*,[†,§]

Institute of Biological Science and Technology, Institute of Nanotechnology, National Chiao Tung University, Hsinchu, Taiwan, and Instrument Technology Research Center, National Applied Research Laboratories (NARL), Hsinchu, Taiwan

Analysis of immobilized enzyme in situ is a crucial step to embed an enzyme onto the planar technology of standard integrated circuit (IC) and microelectromechanical systems (MEMS) for a bioreactor or enzyme-coupled biosensor. A surface reaction limited model, based on a systematized and standardized approach, mathematically derived from mass transfer dynamics and the Michaelis−Menten equation for the measuring the apparent K^*_m (Michaelis−Menten constant) and V^*_{max} (maximum reaction rate per unit surface area of catalyst) of an immobilized enzyme on a planar surface was developed. The derived equations for the kinetic model were simulated and experimentally confirmed. A platform of a microflow bioreactor with a one-sided planar catalytic surface that contained immobilized enzyme was constructed. The microfluidic bioreactor was designed to possess a channel height less than that of the diffusion layer thickness in a semi-infinite diffusion process, and K^*_m and V^*_{max} of rat phenol sulfotransferase (PST) immobilized on the silicon oxide surface were successfully determined in situ. Variation in kinetic constants and the possible differences in performance between free and immobilized PST are discussed.

Many biomolecules, such as membrane proteins, perform their specific biorecognition or biocatalytic activities while they are immobilized on the surface of cells or organelles.[1,2] Artificial technologies also take advantage of immobilized enzymes for a variety of applications such as bioconversion, bioremediation, and biosensors.[3−7] Methods developed for the analysis of the function of biomolecules that move and rotate freely in a homogeneous solution may not be adequate to describe the behavior of immobilized biomolecules. The immobilized enzyme is not distributed evenly and freely in the solution and may have a unique microenvironment for each enzyme molecule. For example, the specific orientation is important for the function of proteins.[8,9] However, free protein in solution can have many orientations, whereas the rotation for an immobilized protein is restricted. Unique kinetic behaviors of membrane-bound enzymes have also been reported.[10,11]

The leading-edge semiconductor devices[12,13] have attracted researches into the emerging fields of biomolecular sensors,[14−17] hybrid (biotic−abiotic) nanomaterials,[18] laboratory-on-a-chip platforms for further biomedical applications,[19] enzyme-coupled biosensors,[20] and novel enzyme-based devices.[21−23] The immobili-

* To whom correspondence should be addressed. E-mail: ysyang@faculty.nctu.edu.tw. Fax: 886-3-5729288.

† Institute of Biological Science and Technology.

‡ Institute of Nanotechnology.

§ NARL.

(1) Branden, C.; Tooze, J. *Intoduction to Protein Structure*, 2nd ed.; Garland: New York, 1999; Chapter 12.

(2) Price, N. C.; Stevens, L. *Fundamentals of Enzymology: The Cell and Molecular Biology of Catalytic Proteins*, 3rd ed.; Oxford University Press: New York, 1999; pp 347−355.

(3) Lamb, S. B.; Lamb, D. C.; Kelly, S. L.; Stuckey, D. C. *FEBS Lett.* **1998**, *431*, 343–346.

(4) Owens, D. R. *Nat. Rev. Drug Discovery* **2002**, *1*, 529–540.

(5) Krenkova, J.; Foret, F. *Electrophoresis* **2004**, *25*, 3550–3563.

(6) Newman, J. D.; Turner, A. P. *Biosens. Bioelectron.* **2005**, *20*, 2435–2453.

(7) Cao, L. *Curr. Opin. Chem. Biol.* **2005**, *9*, 217–226.

(8) Cha, T.; Guo, A.; Zhu, X.-Y. *Proteomics* **2005**, *5*, 416–419.

(9) Talasaz, A.-A. H.; Nemat-Gorgani, M.; Liu, Y.; Stahl, P.; Dutton, R. W.; Ronaghi, M.; Davis, R. W. *Proc. Natl. Acad. Sci. U.S.A.* **2006**, *103*, 14773–14778.

(10) Hardie, G. *J. Histochem. Cytochem.* **1982**, *30*, 1083–1085.

(11) Takakuwa, Y.; Nishino, H.; Ishibe, Y.; Ishibashi, T. *J. Biol. Chem.* **1994**, *269*, 27889–27893.

(12) Fung, S. K. H.; Grudowski, P. A.; Wu, C. H.; Kolagunta, V.; Cave, N.; Yang, C. T.; Lian, S. J.; Adams, V.; Zia, O.; Min, B.; Grove, N.; Chen, K. H.; Liang, W. J.; Lee, D. H.; Huang, H. T.; Cheek, J.; Tuan, H. C. *VLSI Tech. Symp.* **2006**, 1–2.

(13) Bentley, S.; Li, X.; Moran, D. A. J.; Thayne, I. G. *Microelectron. Eng.* **2008**, *85*, 1375–1378.

(14) Neves-Petersen, M. T.; Snabe, T.; Klitgaard, S.; Duroux, M.; Petersen, S. B. *Protein Sci.* **2006**, *15*, 343–351.

(15) Wang, G.; Thai, N. M.; Yau, S.-T. *Biosens. Bioelectron.* **2007**, *22*, 2158–2164.

(16) Hsiao, C.-Y.; Lin, C.-H.; Hung, C.-H.; Su, C.-J.; Lo, Y.-R.; Lee, C.-C.; Lin, H.-C.; Ko, F.-H.; Huang, T.-H.; Yang, Y.-S. *Biosens. Bioelectron.* **2009**, *24*, 1223–1229.

(17) Lin, C.-H.; Hsiao, C.-Y.; Hung, C.-H.; Lo, Y.-R.; Lee, C.-C.; Su, C.-J.; Lin, H.-C.; Ko, F.-H.; Huang, T.-Y.; Yang, Y.-S. *Chem. Commun.* **2008**, 5749–5751.

(18) Ruiz-Hitzky, E., Ariga, K., Lvov, Y. M., Eds. *Bio-inorganic Hybrid Nanomaterials—Strategies, Syntheses, Characterization and Applications*, 1st ed.; Wiley-VCH: Weinheim, Germany, 2007.

(19) Nel, A. L.; Minc, N.; Smadja, C.; Slovakova, M.; Bilkova, Z.; Peyrin, J.-M.; Viovy, J.-L.; Taverna, M. *Lab Chip* **2008**, *8*, 294–301.

(20) Ishige, Y.; Shimoda, M.; Kamahori, M. *Biosens. Bioelectron.* **2009**, *24*, 1096–1102.

(21) Maruccio, G.; Biasco, A.; Visconti, P.; Bramanti, A.; Pompa, P. P.; Calabi, F.; Cingolani, R.; Rinaldi, R.; Corni, S.; Felice, R. D.; Molinari, E.; Verbeet, M. P.; Canters, G. W. *Adv. Mater.* **2005**, *17*, 816–822.

(22) Dzyadevych, S. V.; Soldatkin, A. P.; Korpan, Y. I.; Arkhypova, V. N.; El'skaya, A. V.; Chovelon, J.-M.; Martelet, C.; Jaffrezic-Renault, N. *Anal. Bioanal. Chem.* **2003**, *377*, 496–506.

10.1021/ac802650k CCC: $40.75
Published on Web 03/06/2009

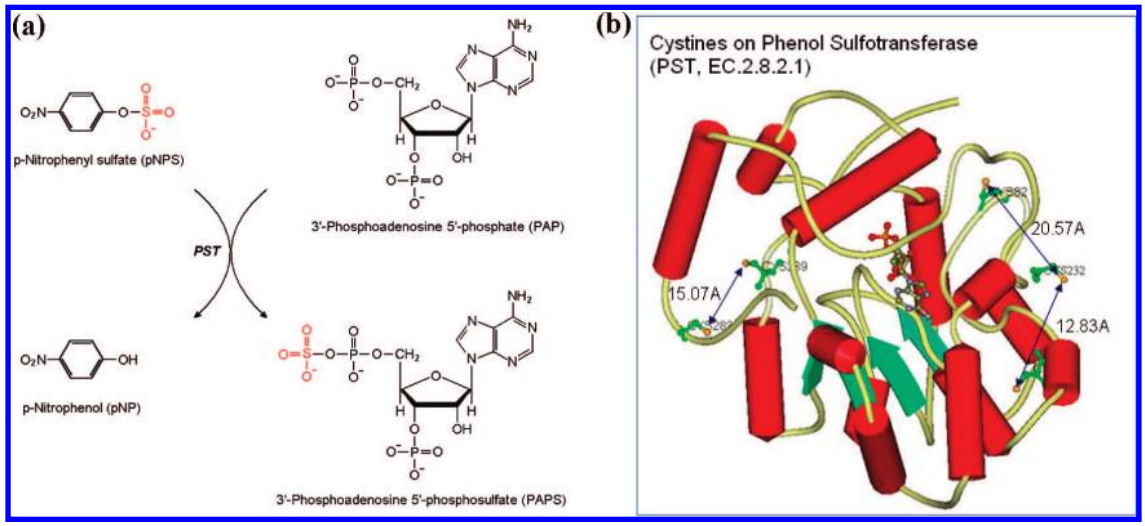

Figure 1. PST-catalyzed sulfuryl group transfer reaction. (a) PAP and pNPS were used as substrates for rat PST. The product, pNP, which gives strong 400 nm absorption in neutral or alkaline solution, served as the reporter molecule for the progress of the enzyme-catalyzed reaction. (b) The structure of rat PST (PDB: 1LS6). Five cystines and PAP are shown with their molecular structures. The distances between nearby cysteines are also indicated.

zation of a variety of biomolecules including proteins and nucleic acids onto silicon-based material is essential for specific biorecognition and electronic signal manipulation required for the biosilicon hybrid devices. How to characterize the reaction kinetics for immobilized enzyme on silicon-based supporting material has become the object of study.[24−28] Kinetic properties of immobilized alkaline phosphatase have been determined in a microfluidic reaction with packed bed.[29] The kinetics of immobilized horseradish peroxidase has been studied using a microfluidic packing reaction[30] and modeling system.[31] With the use of a batch-assay method, the kinetic parameters of immobilized glutathione S-transferase has been determined in porous silicon.[32] The kinetics and transport of this immobilized enzyme have also been simulated by an embedding method in sessile hydrogel drops.[33] Fractal and jamming effects were also used to model the kinetics of heterogeneous enzymatic catalysis.[34] The batch method used for the analysis of immobilized enzyme described above is similar to the conventional method used for the analysis of free enzyme in solution. However, the apparent kinetic values determined may differ significantly from the intrinsic values for the factors that affect diffusion of product, and substrate cannot be ignored in a nonhomogeneous solution. Enzyme kinetics determined in a microfluidic system must consider mass transfer factors that may be significantly affected by the model system used.

To embed biomolecules onto the technology of standard IC (integrated circuit)[35] and MEMS (microelectromechanical systems), the planar surface of Si or SiO_2 is frequently used as the substrate of immobilization. It is very important to be able to determine the kinetics of an enzyme immobilized on these planar surfaces within the microfluidic system in order to evaluate the function of the whole system. So far, there is no such method reported. In this paper, we were developing a novel kinetic model, based on a systematized and standardized approach, for measuring K^*_m (Michaelis−Menten constant) and V^*_{max} (maximum reaction rate per unit surface area of catalyst) of rat phenol sulfotransferase (PST) immobilized on a planar silicon oxide surface within a microfluidic bioreactor. Sulfonation catalyzed by PST in a biological system is a popular and important biotransformation that is involved in detoxification of a broad range of endobiotics and xenobiotics and activation and deactivation of hormones and carcinogens.[36−39] We first tried to derive a mathematical model that can be used to extract the K^*_m and V^*_{max} of an immobilized enzyme in a microfluidic system. To deal with the diffusion effect of enzyme substrate, the ratio of the reaction volume to the catalytic planar surface must be reduced. We built a microfluidic bioreactor with a much smaller channel height than the diffusion layer in a semi-infinite diffusion process according the derived mathematical model. Finally, experiments were performed in order to extract the intrinsic kinetic characteristics of the immobilized enzymes.

THEORETICAL CONSIDERATIONS

Channel Reactor with a One-Sided Planar Catalytic Surface. A model that combined a plug-flow reactor[40] in surface reaction limited conditions[41] was developed to analyze the kinetics

(23) Tseng, G. Y.; Ellenbogen, J. C. *Science* **2001**, *294*, 1293–1294.
(24) Gleason, N. J.; Carbeck, J. D. *Langmuir* **2004**, *20*, 6374–6381.
(25) Fang, S.; Lee, H. J.; Wark, A. W.; Kim, H. M.; Corn, R. M. *Anal. Chem.* **2005**, *77*, 6528–6534.
(26) Wa, C.; Cerny, R. L.; Hage, D. S. *Anal. Chem.* **2006**, *78*, 7967–7977.
(27) Bartolini, M.; Cavrini, V.; Andrisano, V. *J. Chromatogr., A* **2007**, *1144*, 102–110.
(28) Freeman, R.; Gill, R.; Willner, I. *Chem. Commun.* **2007**, *33*, 3450–3452.
(29) Kerby, M. B.; Legge, R. S.; Tripathi, A. *Anal. Chem.* **2006**, *78*, 8273–8280.
(30) Seong, G. H.; Heo, J.; Crooks, R. M. *Anal. Chem.* **2003**, *75*, 3161–3167.
(31) Lilly, M. D.; Hornby, W. E.; Crook, E. M. *Biochem. J.* **1966**, *100*, 718–723.
(32) DeLouise, L. A.; Miller, B. L. *Anal. Chem.* **2005**, *77*, 1950–1956.
(33) Wong, C.-J. An Embedding Method for Simulation of Immobilized Enzyme Kinetics and Transport in Sessile Hydrogel Drops. Ph.D. Thesis, Claremont Graduate University, 2005.
(34) Xu, F.; Ding, H. *Appl. Catal., A* **2007**, *317*, 70–81.
(35) Xiao, H. *Introduction to Semiconductor Manufacturing Technology*; Prentice Hall: Upper Saddle River, New Jersey, 2000.
(36) Duffel, M. W.; Marshall, A. D.; McPhie, P.; Sharma, V.; Jakoby, W. B. *Drug Metab. Rev.* **2001**, *33*, 369–395.
(37) Weinshilboum, R. M.; Otterness, D. M.; Aksoy, I. A.; Wood, T. C.; Her, C.; Raftogianis, R. B. *FASEB J.* **1997**, *11*, 3–14.

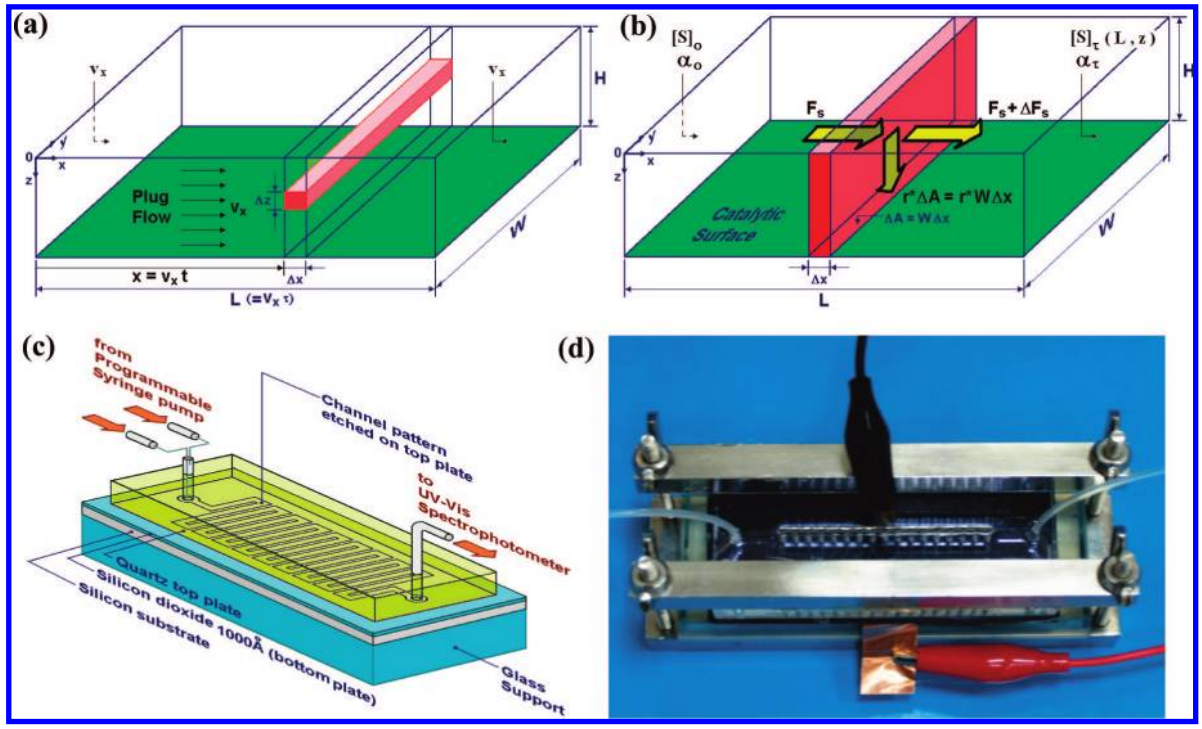

Figure 2. Bioreactor design for the determination of kinetic constants of immobilized enzyme. (a) Rectangular reactor with a catalytic surface on the bottom plate. The channel size is $L \times W \times H$ (where $L \gg W \gg H$). v_x is the velocity of flow between two parallel plates. τ means space time ($\tau = L/v_x$ in this case). (b) The reaction flow in a rectangular bioreactor. The yellow arrows illustrate the material balance of substrate S in the control volume $\Delta x \times W \times H$ at x position, where F_s is molar flow rate of substrate S, (μmol min^{-1}) and r^* is the surface reaction rate on the catalytic surface, (μmol dm^{-2} min^{-1}). $[S]_o$ and $[S]_\tau(L, z)$ are the inlet and the outlet substrate concentrations, respectively, and their corresponding reaction fractions are α_o (= 0, for the common case) and α_τ (for average $\overline{[S]}_\tau$ at $x = L$), respectively. (c) Schematic diagram of the microfluidic reactor. The reactor composes a sandwich structure, the quartz top plate, the Si bottom plate, and the glass supporting plate. The enzyme was immobilized on the SiO_2 surface of the Si bottom plate, and the fluidic channel pattern was etched on the top quartz plate. (d) Photograph of the bioreactor. The reaction solution was pumped into the channel by a programmable syringe pump and eluted to a spectrophotometer for the determination of the concentration of reporter molecules.

of PST-catalyzed reaction (Figure 1). A rectangular channel reactor with proper dimension was designed as shown in Figure 2. This reactor possesses a one-sided catalytic surface with scale size $L \gg W \gg H$ (Figure 2a). We assume that the reaction mixtures flow through the channel at equal velocities and the diffusion effect, as compared to convection in the x-direction, can be neglected (Figure 2b). At steady state, the substrate concentration, determined by diffusion in the z-direction, convection in the x-direction, and consumption at the catalytic surface ($z = H$) is given by eq 1 and the related boundary conditions (BCs) are given by eq 2.

$$v_x \frac{\partial [S]}{\partial x} = D \frac{\partial^2 [S]}{\partial z^2} \tag{1}$$

$$\text{BCs} \begin{cases} [S](0, z) = [S]_o \\ \dfrac{\partial [S]}{\partial z}(x, 0) = 0 \\ -D \dfrac{\partial [S]}{\partial z}(x, H) = k_s [S](x, H) \end{cases} \tag{2}$$

v_x is the velocity of flow between two parallel plates. D is diffusion coefficient of substrate, and k_s (dm min^{-1}) is the rate constant of the surface reaction. Substrate concentration profile of the rectangular reactor, $[S](x, z)$, can be obtained by solving eq 1 coupled with eq 2 and is given as eq 3:

$$[S](x, z) = 4[S]_o \sum_{n=1}^{\infty} \left[\frac{\sin \beta_n}{\sin(2\beta_n) + 2\beta_n} \cos\left(\frac{\beta_n}{H} z\right) \right] \exp\left(-\frac{D\beta_n^2}{v_x H^2} x \right) \tag{3}$$

where eigenvalues, β_n, that fit in eq 3 are given as follows:

$$\tan(\beta_n) = \frac{k_s}{(D/H)\beta_n} \quad \text{or} \quad Da = \beta_n \tan(\beta_n) \tag{4}$$

The dimensionless Damkohler number (Da) in eq 4, is defined as the ratio of the rate constants of the chemical reaction to the mass transfer factor, $Da \equiv k_s/(D/H)$, for this system. $Da \gg 1$ indicates that the system is mass transfer limited, whereas the system becomes surface reaction limited when $Da \ll 1$. In Figure 3a, computer-generated graphs of eq 3 are shown to illustrate substrate concentration profiles at different Da. Average substrate concentration over the cross section on the outlet, $\overline{[S]}_\tau$

(38) Clarke, C.; Thorburn, P.; McDonald, D.; Adams, J. B. *Biochim. Biophys. Acta* **1982**, *707*, 28–37.
(39) Chapman, E.; Best, M. D.; Hanson, S. R.; Wong, C. H. *Angew. Chem., Int. Ed.* **2004**, *43*, 3526–3548.
(40) Levenspiel, O. *Chemical Reaction Engineering*, 3rd ed.; Wiley: New York, 1999.
(41) Welly, J. R.; Wicks, C. E.; Wilson, R. E. *Fundamentals of Momentum, Heat, and Mass Transfer*, 3rd ed.; John Wiley & Sons: New York, 1984.

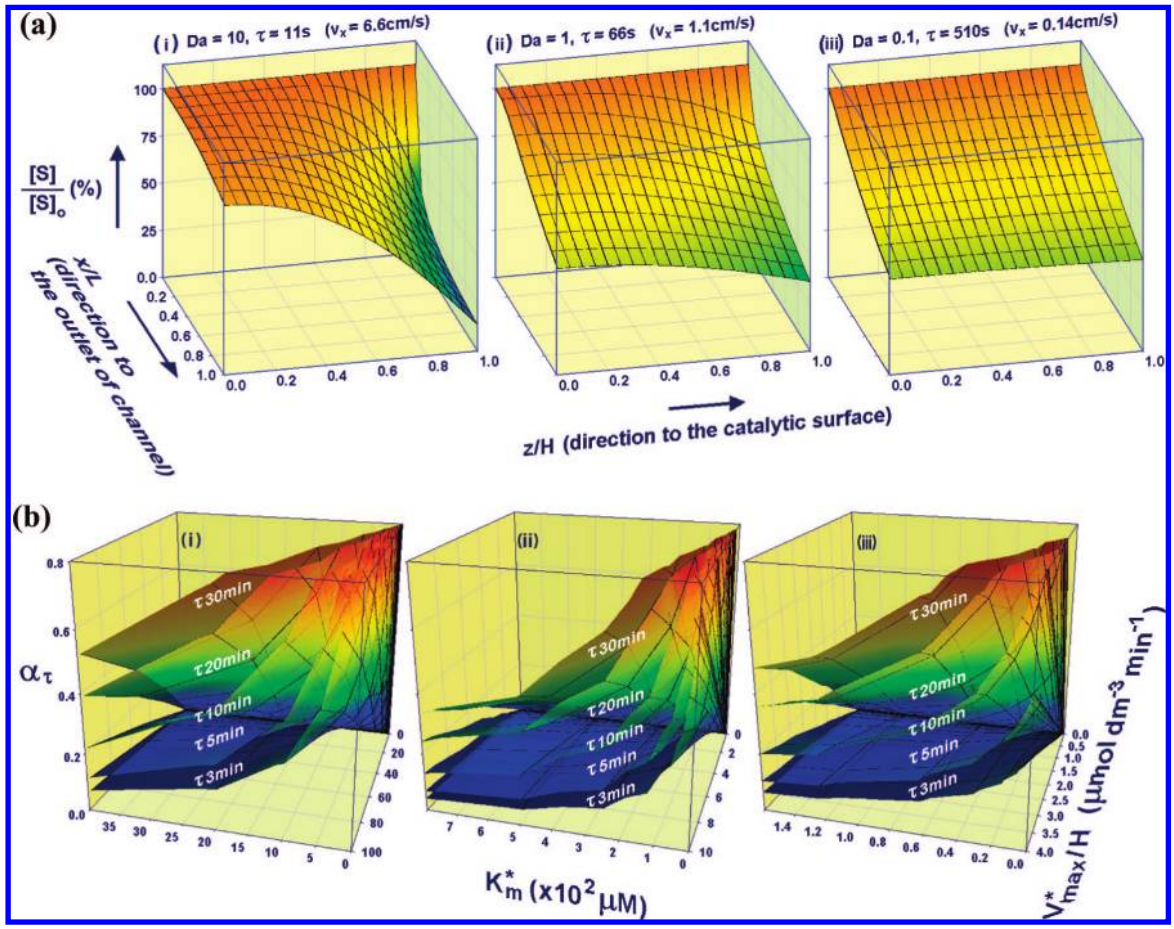

Figure 3. Simulation of reaction conditions and the derivation of kinetic constants. (a) Effect of the Damkohler number on substrate concentration. Substrate concentrations at varied *Da*'s in a rectangular reactor with a catalytic surface on the bottom plate are simulated. The substrate concentration profiles are obtained in a steady-state condition using diffusion coefficient $D = 3.92 \times 10^{-6}$ cm²/s in a rectangular reactor with a catalytic surface at $z = H$ (167 μm). The axes depict the substrate concentration $[S](x, z)$ relative to the inlet substrate concentration $[S]_o$, the distance z from the noncatalytic plate (at $z = 0$) to the catalytic plate (at $z = H$), and the distance x from the inlet ($x = 0$) to the outlet ($x = L$) of the channel as shown in Figure 2. These profiles are created at the conditions of conversion fraction, $\alpha_\tau = 0.5$, that is, $\overline{[S]}_\tau/[S]_o = [S]_{UV}/[S]_o = 0.5$. Parts i, ii, and iii are produced using $Da = 10$, $Da = 1$, and $Da = 0.1$, respectively. (b) Three-dimensional graph of K^*_m and V^*_{max}/H surface. Equation 8 at $[S]_o = 40$ μM is used for the plot. Each surface represents a certain space time, τ. Different scales of K^*_m and V^*_{max}/H are shown in parts i, ii, and iii.

(at $x = L$), is equal to the outlet substrate concentration $[S]_{UV}$ detected by UV−vis spectrophotometer; therefore

$$\overline{[S]}_\tau = \frac{4[S]_o}{H}\sum_{n=1}^{\infty}\left[\frac{\sin\beta_n}{\sin(2\beta_n) + 2\beta_n}\right]\exp\left(-\frac{D{\beta_n}^2\tau}{H^2}\right)\int_0^H \cos\left(\frac{\beta_n z}{H}\right) dz = [S]_{UV} \quad (5)$$

where space time τ is the time required to process the volume of reaction mixture in the reactor. Let α_τ be the average reaction conversion fraction at the outlet, $\alpha_\tau \equiv ([S]_o - \overline{[S]}_\tau)/([S]_o) = ([S]_o - [S]_{UV})/([S]_o)$, and eq 5 becomes eq 6.

$$\alpha_\tau = 1 - \frac{[S]_{UV}}{[S]_o} = 1 - 4\sum_{n=1}^{\infty}\frac{\sin^2\beta_n}{\beta_n[\sin(2\beta_n) + 2\beta_n]}\exp\left(-\frac{D{\beta_n}^2\tau}{H^2}\right) \quad (6)$$

By coupling eqs 4 and 6, the magnitude of *Da* can be evaluated by numerical analysis method (detailed analysis and prediction of *Da* are given in the Supporting Information) when the substrate conversion α_τ is known. The height, H, of the channel, the space time, τ, and the substrate concentration at inlet of the channel, $[S]_o$, can be set as experimental parameters in eqs 4 and 6. The substrate concentration at the outlet of the channel, $[S]_{UV}$, is a measurable value. In addition, the liquid mass diffusivity of the substrate, D, can be predicted by experimental methods and theoretical formula.[41,42] The diffusion coefficient, D, of most small molecules in a dilute solution has 10^{-6} cm²/s order.[43]

Surface Reaction Limited Model. As shown in Figure 3a, part iii, the substrate concentration is nearly uniform in the z-direction under $Da = 0.1$ condition based on the channel reactor with a one-sided planar catalytic surface as described above. In this condition, $[S]$ becomes a function of x only and can be used to derive an equation to extract the kinetic constant of the immobilized enzyme.

In a steady-state condition (at a constant flow rate), the enzyme reaction rate on the catalytic surface is

(42) Wilke, C. R.; Chang, P. *AIChE J.* **1955**, *1*, 264–270.
(43) Lide, D. R. *CRC Handbook of Chemistry and Physics*, 84th ed.; CRC Press: Boca Raton, FL, 2004.

$$r^*(x) = \frac{V^*_{max}[S](x,H)}{K^*_m + [S](x,H)} \approx \frac{V^*_{max}[S](x)}{K^*_m + [S](x)} \quad (7)$$

where V^*_{max} is maximum reaction rate per unit surface area of catalyst (μmol dm^{-2} min^{-1}), K^*_m is the Michaelis−Menten constant (μmol dm^{-3}) for immobilized enzymes on the planar surface. Substituting eq 7 into the mass balance of substrate S gives eq 8:

$$\tau = \frac{-K^*_m}{V^*_{max}/H} Ln(1 - \alpha_\tau) + \frac{[S]_o}{V^*_{max}/H}\alpha_\tau \quad (8)$$

A computer-generated plotting based on eq 8 at a certain $[S]_o$ is shown in Figure 3b. The optimum value of $-K^*_m/(V^*_{max}/H)$ and $[S]_o/(V^*_{max}/H)$ can be found based on certain parameters, including $[S]_o$, H, and the set of experimental data between space time, τ, and conversion fraction, α_τ. Therefore, K^*_m and V^*_{max} can be evaluated by regression analysis using eq 8.

If reaction conversion fraction, α_τ, is smaller than 1%, and $[S]_o$ is much greater than K^*_m, then eq 8 can be degenerated as follows:

$$\alpha_\tau \approx \left(\frac{V^*_{max}}{H}\right)\left(\frac{\tau}{[S]_o}\right) \quad (\text{for } [S]_o \gg K^*_m) \quad (9)$$

This means that the whole immobilized enzymes (from the entrance to the outlet of reactor shown in Figure 2, parts a and b, as a green surface) are under saturating substrate conditions. Under this degenerated condition, eq 9 provides us the opportunity to determine the simultaneous value of V^*_{max}/H. Simultaneous determination of enzyme activity is important because the inactivation of immobilized enzyme is generally expected (Figure 4).

EXPERIMENTAL SECTION

Surface Modification on the Silicon Wafer. P-type Si(100) wafers (14−21 Ω·cm, MEMC, Missouri) with 15 cm diameter, on which 100 nm oxide layers were grown using wet oxidation with a gas mixture of hydrogen (8000 cm^3/min) and oxygen (5000 cm^3/min) at 978 °C, were cut into 4 × 8 cm^2 pieces of samples to serve as a supporting material for enzyme immobilization. Prior to immobilization, the piece of oxidized silicon wafer was carefully cleaned in the piranha solution, H_2SO_4 and H_2O_2 (volume ratio is 3:1), twice, each time at above 85 °C for 30 min. It should be noted that the cleaning solution is very corrosive and dangerous. After rinsing with pure water and drying, the sample was immersed in the (3-aminopropyl)-triethoxysilane (APTES, Sigma-Aldrich, Missouri) solution to proceed the silanization reaction for 30 min at room temperature to create an amine-functional surface (Supporting Information Figure S2). The APTES solution was prepared by the following procedures: (1) mixing pure water with acetone (volume ratio is 5:1), (2) adjusting the pH value of the above solvent to 3.5 by 1 M HCl, and (3) preparing the 5% APTES solution by diluting with the above solvent. Following the APTES treatment, the silicon wafer was rinsed with pure water thoroughly. Then, the treated silicon wafer was baked at 120 °C for 30 min to complete the Si−O bond formation.[44] To create a maleimide group for the immobilization of enzyme through its sulfhydryl group, sulfosuccinimidyl 4-(*N*-maleimidomethyl)-cyclohexane-1-carboxylate (sulfo-SMCC, Sigma-Aldrich) was used to link to the amino group of APTES on the surface of the silicon wafer (Supporting Information Figure S2). The 0.5 mM sulfo-SMCC linker solution was prepared by dissolving sulfo-SMCC into 50 mM sodium borate buffer (Sigma-Aldrich), and then the linker solution was dipped onto the silanized surface of the sample for 1 h at room temperature. Finally, the surface was extensively rinsed with water and dried with nitrogen gas.

Reactor System and Enzyme Immobilization. The microfluidic channel of the reactor shown in Figure 2, parts c and d, is composed of two plates. The bottom plate was the silicon wafer on glass support. The silicon surface was modified with APTES and maleimide as described above. The top plate, made of quartz, contained a tortuous fluidic guide on its surface formed by etching. The fluidic channel was 72.6 cm long, 0.194 cm wide, and 167 μm deep. To avoid leakage during pumping operation, the edges between the two plates were sealed with glue and the two plates were tightly clamped together using a screwed clamp holder. The enzyme solution (200 μg/mL rat PST, EC.2.8.2.1, in 0.1 M sodium phosphate buffer at pH 7.0) prepared according to published procedure[45,46] was pumped into the microfluidic system by a programmable syringe pump (KD Scientific, KDS260P) at space time τ = 0.5 min (equivalent to 28.2 mL/h or v_x = 2.4 cm/s) and stopped to incubate for 15 min at room temperature. Next, 50 mM 2-mercaptoethanol solution (in 50 mM sodium phosphate buffer at pH 7.0) was pumped into the microfluidic system and stopped to incubate for 8 min at room temperature. Finally, 50 mM sodium phosphate buffer was pumped into the microfluidic system to wash away the residual 2-mercaptoethanol solution. Reactions involved in the surface modification and the immobilization of rat PST are shown in Supporting Information Figure S-2.

Enzyme Assay. Two different concentrations of 3′-phosphoadenosine 5′-phosphate (PAP), 400 and 2 μM, were used to create saturating and nonsaturating substrate condition, respectively, for the immobilized PST-catalyzed reaction. The PAP concentrations used were determined according to the K_m of free rat PST[45,46] and eq 8 in a surface reaction limited model. The reaction mixtures for immobilized rat PST contained PAP (400 or 2 μM) and 20 mM *p*-nitrophenyl sulfate (pNPS) in 100 mM 1,3-bis[tris(hydroxymethyl)methylamino]propane buffer at pH 7. Injection of the reaction mixtures into the reactor was controlled by an automatic pumping system and operated at the desired flow rate to have space time, τ, at 1, 2, 4, or 8 min. The output solution was directed into a quartz flow cell mounted in the UV−vis spectrophotometer (Hitachi UV−vis-3300, Tokyo, Japan) for pNP detection at 400 nm (Figure 1).

RESULTS AND DISCUSSION

Development of the Surface Reaction Limited Model for the Derivation of K^*_m and V^*_{max}. Computer-generated figures (Figure 3) and equations derived (eqs 8 and 9) based on a

(44) Sato, T.; Brown, D.; Johnson, B. F. G. *Chem. Commun.* **1997**, 1007–1008.

(45) Yang, Y.-S.; Tsai, S.-W.; Lin, E.-S. *Chem.-Biol. Interact.* **1998**, *109*, 129–135.

(46) Lin, E.-S.; Yang, Y.-S. *Anal. Biochem.* **1998**, *264*, 111–117.

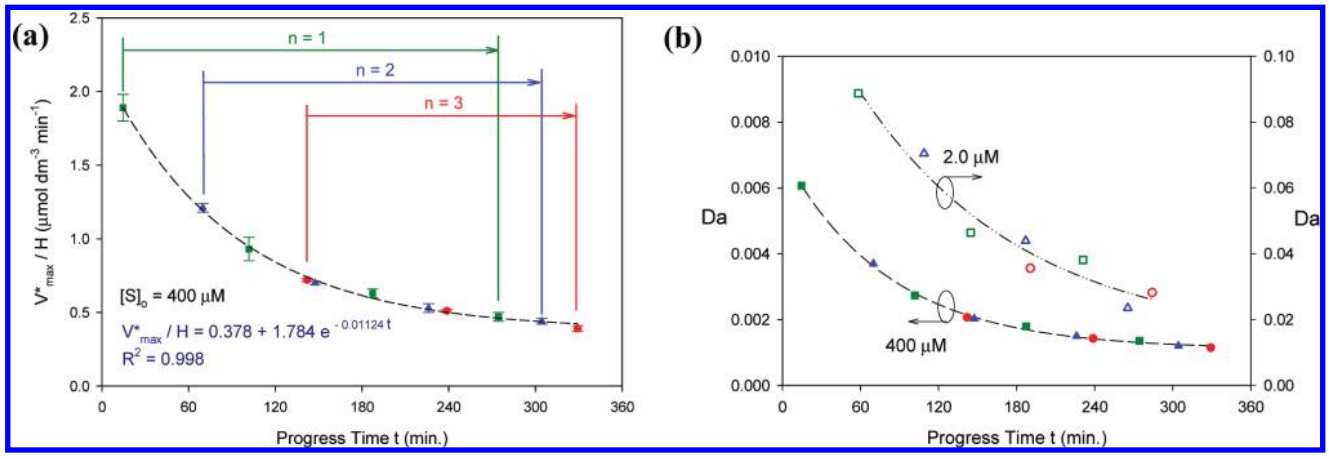

Figure 4. Stability of PST and its effect on the Damkohler number. (a) Deactivation curve of rat PST under saturating substrate condition. High substrate concentration (400 μM PAP) was used to give the characteristic curve of rat PST determined according to eq 9. Three data sets, dark-green rectangles, blue triangles, and red circles, were collected at different times (simultaneously and 1 and 2 h) after immobilization of PST. (b) Effect of substrate concentration and enzymatic activity on *Da*. Typical *Da* was obtained at space time $\tau = 4$ min. The curves decayed gradually due to the deactivation of enzyme. Dark-green squares, blue triangles, and red circles were recorded independently at different times after immobilization of PST. The upper (open symbols) and lower lines (solid symbols) represent low (2.0 μM) and high (400 μM) substrate concentration conditions, respectively.

rectangular bioreactor (Figure 2) demonstrated that a surface reaction limited model can be used to obtain kinetic constants of immobilized enzyme in an appropriate reaction condition. Figure 3a illustrates three types of reaction kinetics based on the same average conversion fraction $\alpha_\tau = 50\%$ across the outlet area (Figure 2). Dimensionless *Da*, defined as the ratio of the rate constants of the chemical reaction to the mass transfer factor, is used to distinguish the three types of reaction kinetics. The mass transfer limited condition ($Da \gg 1$) indicates that the perpendicular diffusion rate is much slower than the rate of reaction on the catalytic surface (as shown in Figure 3a, part i, $Da = 10$). The transition condition ($Da \approx 1$) indicates that the diffusion rate is comparable to the surface reaction rate (as shown in Figure 3a, part ii, $Da = 1$). The surface reaction limited condition ($Da \ll 1$) shown in Figure 3a, part iii, indicates that the perpendicular diffusion rate is much higher than the surface reaction rate. At $Da = 0.1$ (Figure 3a, part iii), the concentrations of substrate and products can be evenly distributed on the z (or H) direction (Figure 2).

Figure 3b illustrates computer-generated curved surfaces under the $Da \ll 1$ condition at certain space times according to eq 8. One set of K^*_m and V^*_{max}/H can be obtained on the curved surface at a specific substrate concentration and space time. This indicates that, following the regression analysis, the K^*_m and V^*_{max} of the immobilized enzyme can be obtained using different flow rates (or space time) to determine the rate of substrate conversion to product in the bioreactor. The curve surfaces shown in Figure 3b were simulated at $[S]_o = 40$ μM with space time $\tau = 3$, 5, 10, 20, and 30 min. Parts i, ii, and iii of Figure 3b are shown with different scales of K^*_m and V^*_{max}/H to reveal the variation of the curve surfaces. In order to obtain a better K^*_m and V^*_{max}/H following regression analysis, it is desirable that α_τ (converted from space time, τ) is chosen where curve surfaces vary more drastically with respect to K^*_m and V^*_{max}/H axes shown in Figure 3b. For example, as shown in Figure 3b, part iii, it would be suitable to determine the kinetic constants of an immobilized enzyme with $K^*_m < 40$ μM and $V^*_{max}/H < 3$ μM min^{-1} using the reaction condition of $[S]_o = 40$ μM, $\tau = 3$, 5, 10, 20, and 30 min. However, this reaction condition is inappropriate for an immobilized enzyme with $K^*_m > 600$ μM and $V^*_{max}/H = 2-10$ μM min^{-1} (Figure 3b, part ii), because at this region, the variation on the curve surface is small and thus even small errors produced by the α_τ data determination may significantly affect the values of K^*_m and V^*_{max}/H following regression analysis. In other words, after K^*_m and V^*_{max}/H were obtained experimentally, Figure 3b can provide us to check for the accuracy of these values and, if necessary, further guide us to select appropriate experiment parameters, set of space times, for more accurate measurement of K^*_m value.

Stability and V^*_{max}/H of Immobilized Enzyme on a Planar Si Surface. The stability of the enzyme is a concern for all biorelated applications when it is used as a catalyst. It is important that the stability and activity of the immobilized enzyme can be monitored or predicted during the whole reaction process. It is reasonable to assume that the loss of total enzyme activity is due to the inactivation of part of the protein molecules. That is, each enzyme molecule is either fully active or completely dead and its K_m and k_{cat} remain the same for each active enzyme molecule. The determination of V^*_{max}/H can be achieved easily using eq 9 degenerated from eq 8 under saturating substrate condition. As shown in Figure 4a, V^*_{max}/H's were obtained experimentally at several progress times after immobilization in a surface reaction limited condition at high substrate concentration. The decrease in total activity indicated inactivation of enzyme following immobilization. Three sets of immobilized PST whose activities were determined at different stages following immobilization all followed the same deactivation pattern shown in Figure 4a. The deactivation curve indicates that the activity of PST can be predicted, and the resulting V^*_{max}/H obtained can be normalized at any given time following its immobilization on the reactor surface. The decay curves (Figure 4) were used to normalized V^*_{max}/H at various progress times and to derive K^*_m at low substrate concentration (Figure 5).

To ensure that the required condition, $Da \ll 1$, can be satisfied in this study for the surface reaction limited model, the *Da* in

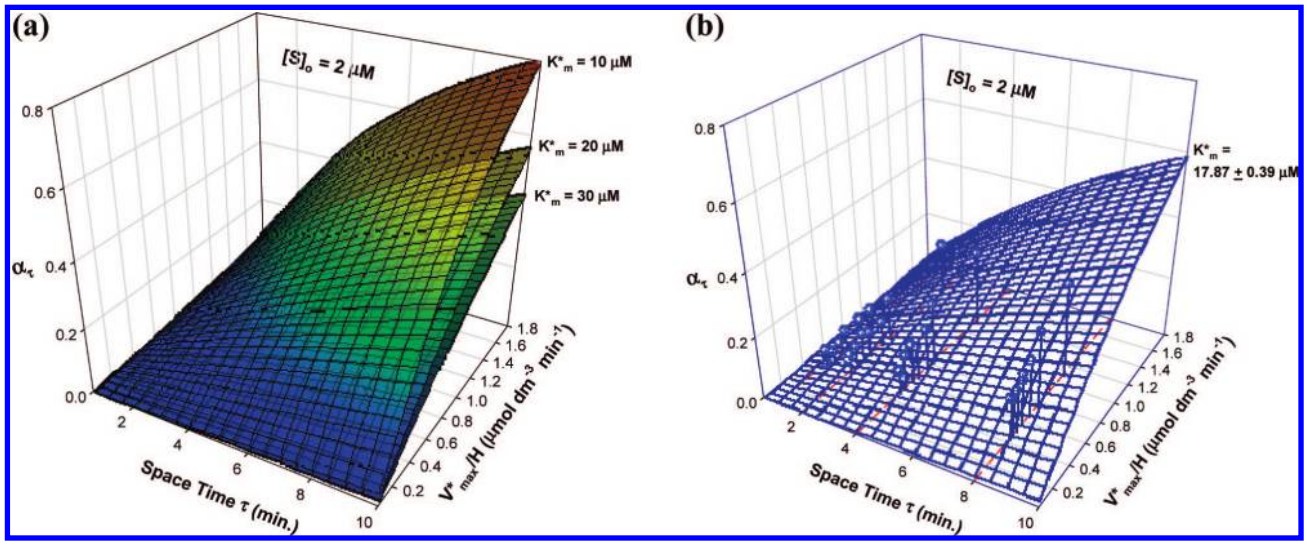

Figure 5. Curved surfaces of K^*_m in the space of $\tau - V^*_{max}/H - \alpha_\tau$. (a) Computer-generated plots of eq 8 at moderate low concentration of substrate. Each K^*_m curved surface clearly separates one another at comparable low substrate concentration. (b) K^*_m curved surface produced by experimental data. The curved surface of $K^*_m = 17.87 \pm 0.39$ μM was generated through regression analysis of experimental data at $[S]_o = 2$ μM.

Scheme 1. Step-by-Step Consideration for the Determination of K^*_m and V^*_{max} of an Immobilized Enzyme on a Planar Surface Using the Surface Reaction Limited Model

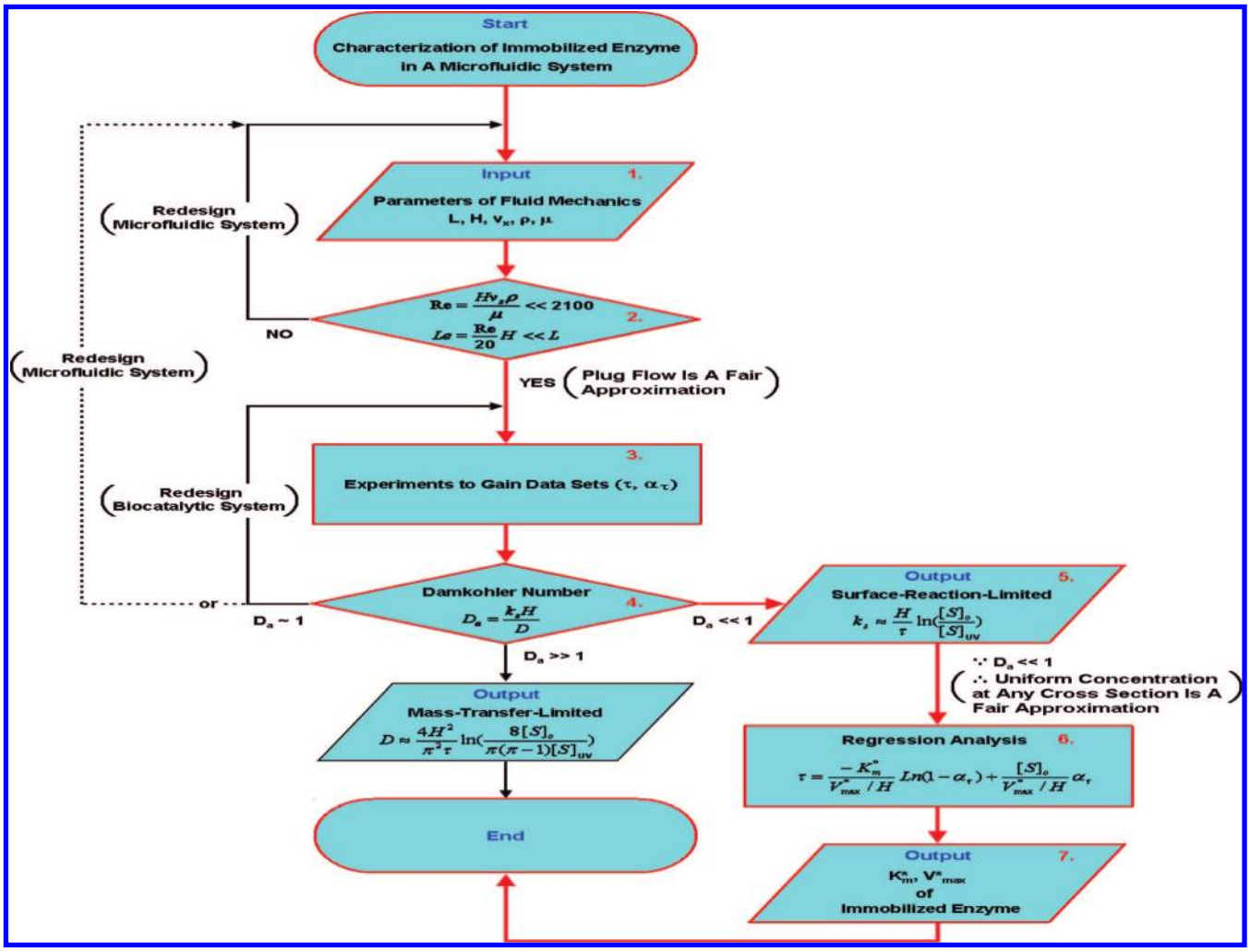

low and high substrate concentration, respectively, are shown in Figure 4b. Both the substrate concentration and the decay of enzyme activity following immobilization at various progress times significantly affected the *Da*. This observation is expected for the catalytic reaction on the planar surface is to be affected by the amount of active enzyme and substrate concentration. This

indicates that the relative substrate consumption on the reaction surface was more significant than those perpendicular from the reaction surface. At $[S]_o = 2\ \mu M$, the *Da* was about an order higher than that of $[S]_o = 40\ \mu M$. However, all the *Da* shown in Figure 4b are lower than 0.1. Under such condition, the concentration profile in the z (or H) direction can be considered constant and satisfies the requirement for the surface reaction limited model shown in Figure 3a, part iii.

Determination of K^*_m(PAP) through Regression Analysis. As shown in Figure 5a, a specific curved surface of a certain K^*_m can be obtained according to eq 8 by giving any set of values τ, V^*_{max}/H, and α_τ. The computer-generated Figure 5a also shows that K^*_m can be determined through a series of τ and V^*_{max}/H values when $[S]_o$ and K^*_m values are in the same order of magnitude. Experimental data, using $[S]_o = 2\ \mu M$, were obtained and fit into eq 8 as shown in Figure 5b. Regression analysis of the experimental data matched very well with the curved surface of $K^*_m(PAP) = 17.87 \pm 0.39\ \mu M$. The original V^*_{max}/H (PST activity just after immobilization) was determined as 2.16 μM/min (or $V^*_{max} = 0.36$ pmol/min/dm^2) according to Figure 4a. The amount of PST per unit area estimated by atomic force microscopy (AFM) (detailed procedures are given in Supporting Information) was about 0.38 pmol/dm^2, which gives $V^*_{max} = 27.2$ nmol/min/mg. The K_m(PAP) and V_{max} of free PST in a homogeneous system were $4.10 \pm 0.26\ \mu M$ and 295 ± 3 nmol/min/mg, respectively. The K^*_m(PAP) of immobilized PST was significantly higher than that of the free enzyme. It is reasonable for immobilized enzyme to exhibit a higher K^*_m because, as compared to free enzyme in solution, it decreases its degree of freedom and may be difficult to maintain its flexible and proper conformation in a more stressful environment. Thus, the affinity of the substrate with enzyme may be weakening and higher substrate concentration may be needed to give the maximum enzyme activity as compared to that of free enzyme in solution. The V^*_{max} of immobilized PST was about 10-fold less than that of free PST. Since PST is a cytosolic enzyme, it would not be surprising that its activity was found to be considerably lower following immobilization. Other factors may also affect PST activity such as the orientation of PST immobilization, the formation of monomer following immobilization, and the change of the PST environment due to PST immobilization on the silicon oxide surface. All these possible factors may be studied one by one in the near future. Multipoint immobilization is possible since there are five cysteines in a rat PST (Figure 1b). This may lead to the distortion of tertiary structure of immobilized PST and therefore to a decrease in its activity. Different orientations, conformations, and degrees of freedom can be expected following PST immobilization. Therefore the kinetic parameters of immobilized PST determined in this research should be considered the average behavior of the enzyme in various conditions. This research focused on the establishment of a measurement platform and model. In the near future, we plan to use site-directed mutagenesis to produce PST with a single free cystein to clarify the immobilizing issue and to study the redox-regulating mechanism of immobilized rat PST.

CONCLUSIONS

We have developed a novel scheme for the determination of kinetic parameters of an immobilized enzyme on a planar surface through a systematized and standardized consideration shown in Scheme 1. This scheme can be followed step-by-step to evaluate kinetic properties of immobilized enzyme in situ based on a surface reaction limited experimental condition. It is important because a standard scheme is necessary to compare the performance of immobilized enzyme operated by different research groups. In the real-life application, the catalytic activity can be significantly increased by immobilizing enzyme on all walls surrounding the microfluidic channel.

ACKNOWLEDGMENT

The research was financially supported by the National Science Council, Taiwan (97-2321-B-009-001 and 97-2627-B-009-009).

SUPPORTING INFORMATION AVAILABLE

Additional information as noted in text. This material is available free of charge via the Internet at http://pubs.acs.org.

Received for review December 16, 2008. Accepted February 13, 2009.

AC802650K